

University of California - Davis
University of Wisconsin - Madison

UCD-98-4
MADPH-98-1033
hep-ph/9801317
January, 1998

Measuring the Coupling of a Higgs Boson to ZZ at Linear Colliders

J.F. Gunion¹, T. Han^{1,2} and R. Sobey¹

¹*Davis Institute for High Energy Physics
University of California, Davis, CA 95616*

²*Department of Physics, 1150 University Avenue
University of Wisconsin, Madison, WI 53706*

Abstract

We study the achievable accuracy for measuring the ZZh coupling (g_{ZZh}^2) of a light ($m_h \lesssim 140$ GeV) SM-like Higgs boson at $e^\pm e^-$ linear colliders in a model-independent way. At a 500 GeV linear collider, including the (dominant) ZZ -fusion process dramatically increases the precision that can be achieved using only the Zh associated production process; after combining, errors of $\lesssim 5\% - 8\%$ are achieved for NLC detector parameters and an integrated luminosity of 200 fb^{-1} . This is to be compared to errors of $\lesssim 5\%$ obtained when the same integrated luminosity is accumulated at $\sqrt{s} = m_Z + \sqrt{2} m_h$ (for which the Zh process is dominant).

1 Introduction

Once a neutral Higgs boson (h) is discovered, measuring its coupling to Z bosons (g_{ZZh}) is of fundamental importance.¹ It is this coupling which most directly reflects the role of the h in electroweak symmetry breaking. In the minimal Standard Model (SM), where the Higgs sector consists of a single Higgs doublet field, there is only one physical Higgs boson eigenstate, with coupling $g_{ZZh} = gm_Z/\cos\theta_W$, where g is the $SU(2)$ coupling and θ_W is the weak mixing angle. In contrast, in a theory with many scalar doublets and/or singlets, the ZZ couplings of the individual neutral Higgs bosons (h_i) are generally reduced in magnitude, but must obey the sum rule [3] $\sum_i g_{ZZh_i}^2 = [gm_Z/\cos\theta_W]^2$. The sum rule becomes still more complicated if triplet Higgs representations are present. Precise determination of g_{ZZh} for each and every observed h will therefore be crucial to knowing whether or not we have found all the Higgs bosons that participate in electroweak symmetry breaking and to understanding the full structure of the Higgs sector.

¹For recent reviews of Higgs boson phenomenology, see *e.g.*, Refs. [1, 2].

In e^+e^- collisions, the dominant Higgs boson production diagrams involving the ZZh coupling are of two types:

$$e^+e^- \rightarrow Zh \quad (1)$$

$$e^+e^- \rightarrow e^+e^-Z^*Z^* \rightarrow e^+e^-h. \quad (2)$$

There is (constructive) interference of the amplitude for $e^+e^- \rightarrow Zh \rightarrow e^+e^-h$ with that for (2). However, it is desirable both for simplicity and in order to maximize experimental accuracy for the g_{ZZh} determination to impose cuts such that this interference is very small; the Zh (1) and ZZ -fusion (2) amplitudes can then be considered as leading to effectively independent production processes.² If the linear collider is run in the e^-e^- mode, the only source of h production is from ZZ -fusion $e^-e^- \rightarrow e^-e^-h$ [5].

Processes (1) and (2) have quite different characteristics. For a lighter Higgs boson and lower center of mass energy (\sqrt{s}) process (1) dominates (with a maximal cross section at $\sqrt{s} \sim m_Z + \sqrt{2} m_h$), while for a heavier Higgs boson or higher \sqrt{s} , process (2) becomes more important (the cross section increasing logarithmically with \sqrt{s}). This is shown in Figure 1, where we present the total cross section for $e^+e^- \rightarrow e^+e^-h$ (solid) as a function of \sqrt{s} for several Higgs boson masses, $m_h = 80, 120, 160$ and 200 GeV. Dashed curves present the contribution only from $e^+e^- \rightarrow Zh$ with $Z \rightarrow e^+e^-$. Note that the ZZ fusion cross section becomes larger than that of Zh for $\sqrt{s} > 300$ GeV.

In both the Zh and ZZ -fusion channels, the Higgs signal can be easily detected for $m_h \lesssim (0.7 - 0.8)\sqrt{s}$ by reconstructing the Higgs mass peak via the h decay products. However, in order to measure the ZZh coupling in a *model-independent* manner (*i.e.* independent of the h 's branching ratio to any particular channel), it will be crucial to identify the Higgs signal through the “recoil mass” variable,

$$M_{\text{rec}}^2 = s + M_{\ell\ell}^2 - 2\sqrt{s}(E_{\ell^+} + E_{\ell^-}), \quad (3)$$

where $M_{\ell\ell}$ is the invariant mass of the final state lepton pair and the E_ℓ are the lepton energies in the c.m. frame; here, $\ell = e, \mu$ is possible for process (1)³ while only $\ell = e$ is relevant for process (2). Due to detector resolution effects, M_{rec} will display a peaked distribution of finite width, much broader than the physical width of a light Higgs boson, centered about m_h . If we can measure the inclusive cross

²Nonetheless, our calculations will always employ the full SM matrix elements [4], including all interfering diagrams, for any particular signal final state. Full matrix elements are also employed for background processes contributing to any particular final state. However, interference between the signal and background is neglected; this is an excellent approximation when considering a very narrow light Higgs boson.

³One could also consider reconstructing an M_{rec} peak using the $Z \rightarrow q\bar{q}$ (hadronic) decays in Eq. (1) in order to increase the signal statistics. However, the energy/momentum resolution for jets is much worse than for leptons and the backgrounds in the hadronic decay channels are larger, implying a less sharp signal peak above background. Thus, we will consider only the leptonic modes.

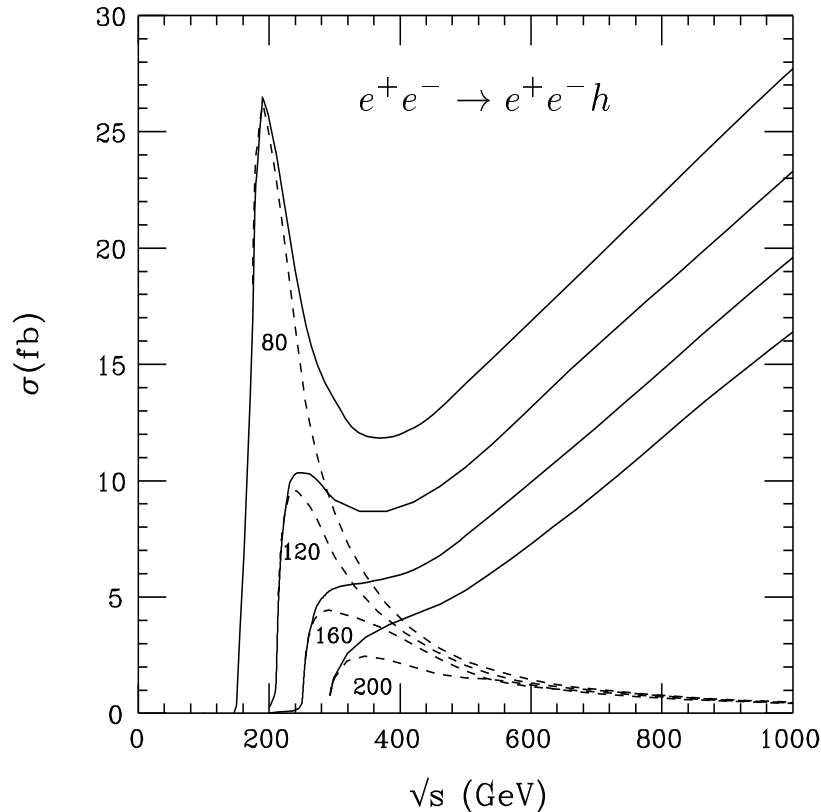


Figure 1: Total cross section for $e^+e^- \rightarrow e^+e^-h$ (solid) as a function of \sqrt{s} for $m_h = 80, 120, 160$ and 200 GeV. Dashed curves present the contribution only from $e^+e^- \rightarrow Zh$ with $Z \rightarrow e^+e^-$.

section associated with the M_{rec} peak in such a way that there is small sensitivity to the h decay, then we can obtain a direct determination for the ZZh coupling g_{ZZh} .

Since we allow the Higgs to decay to anything, our background is composed of many processes. For $\ell = e$, for example, we must consider all processes of the type:

$$e^+e^- \rightarrow e^+e^-X, \quad (4)$$

with $X = \ell^+\ell^-, \tau^+\tau^-, \nu\bar{\nu}$ and $q\bar{q}$.

Many analyses of the process (1) in the inclusive M_{rec} context have appeared in the literature; see, for example, [6, 7, 8, 2, 9] and references therein. However, process (2) has received limited attention [2, 10]. In particular, complete background computations for the inclusive signal are given for the first time in the present paper.

The rest of the paper is organized as follows. In Sec. 2 we explore in detail the precision achievable for the measurement of g_{ZZh}^2 (assuming a SM-like h) by the

processes (1) and (2), and comment on the $e^-e^- \rightarrow e^-e^-h$ ZZ -fusion production mode. Section 3 summarizes our results.

2 Procedures and accuracies for measuring g_{ZZh}^2

In order to reconstruct the signal peak in M_{rec} via Eq. (3), we must assure that the charged leptons are detected. Thus, we impose the following “basic” acceptance cuts

$$|\cos \theta_\ell| < 0.989, \quad p_T(\ell^\pm) > 15 \text{ GeV}, \quad p_T(\ell^+\ell^-) > 30 \text{ GeV}, \\ M_{\ell\ell} > 40 \text{ GeV}, \quad \text{and} \quad M_{\text{rec}} > 70 \text{ GeV}. \quad (5)$$

The polar angle cut roughly simulates the detector acceptance for a beam hole of 150 mrad [8], and the cut on $M_{\ell\ell}$ is imposed in order to suppress events from photon conversion.

The sharpness of the reconstructed M_{rec} peak is determined by the momentum/energy resolution for the charged leptons. The energy of an electron (but not that of a muon) can be measured in the electromagnetic calorimeter. The momentum of either a muon or an electron can be determined from a tracking measurement of its curvature in the magnetic field of the detector. We consider two possibilities for the energy resolution of the electromagnetic calorimeter:

$$\text{I: NLC/EM} \quad \Delta E/E = 12\%/\sqrt{E} \oplus 1\%;$$

$$\text{II: CMS/EM} \quad \Delta E/E = 2\%/\sqrt{E} \oplus 0.5\%.$$

where \oplus denotes the sum in quadrature and E is in GeV. Case I is that currently discussed for the NLC electromagnetic calorimeter [8]; case II is that of the CMS lead-tungstate crystal [11]. We also consider two possibilities for the momentum resolution from tracking:

$$\text{III: NLC/tracking} \quad \Delta p/p = 2 \times 10^{-4}p \oplus 1.5 \times 10^{-3}/\sqrt{p} \sin^2 \theta;$$

$$\text{IV: SJLC/tracking} \quad \Delta p/p = 5 \times 10^{-5}p \oplus 10^{-3},$$

with p in GeV. Case III is that specified for the typical NLC detector in [8] and case IV is that quoted for the “super-JLC” (SJLC) detector design [12].

It is important to note that for an electron the tracking determination of its momentum is not statistically independent of the electromagnetic calorimeter measurement of its energy. Thus, the two measurements cannot be combined; one should use whichever measurement provides the best result. In order to provide a clean comparison of the different possibilities, we will present results in which we analyze all events using either the calorimeter energy measurement or the tracking measurement; *i.e.* we do not choose the best measurement on an event-by-event basis.

It is useful to compare the fractional resolutions, $r \equiv \Delta E/E$ ($E \sim p$ for $\ell = e, \mu$), for the different cases to one another as a function of energy/momentum. Using $\theta = 90^\circ$ in III, one finds that $r_{\text{III}} > r_{\text{I}}$ for any $E > 70$ GeV (lower E for θ in the forward or backward direction) and that $r_{\text{I}} > r_{\text{IV}} > r_{\text{II}}$ for $E > 100$ GeV. At $\sqrt{s} = 500$ GeV, lepton energies above 100 GeV are typical for the light Higgs masses studied here; then, NLC/tracking will not be useful for an electron, whereas SJLC/tracking might be, depending upon the EM calorimeter. Since the muon energy/momentum can only be measured by tracking, NLC/tracking will result in the $Zh \rightarrow \mu^+\mu^-h$ channel having a poorer signal to background ratio than either the $Zh \rightarrow e^+e^-h$ or the ZZ -fusion e^+e^-h channel. On the other hand, if the machine energy is lower, *e.g.* near the peak in the Zh cross section for small m_h , electron energies are smaller, and for the majority of events the NLC/tracking measurement of the electron energy is competitive with the NLC/EM measurement. This will be apparent from the figures in the next section.

To suppress the SM background more effectively and for physics clarity, it is beneficial to divide the study into the two natural categories: the Zh associated production and ZZ fusion processes.

2.1 $e^+e^- \rightarrow Zh \rightarrow e^+e^-h$ and $\mu^+\mu^-h$

We first discuss a linear collider with $\sqrt{s} = 500$ GeV. In order to isolate the Zh class of events we require

$$|M_{\ell\ell} - m_Z| < 10 \text{ GeV} , \quad |\cos \theta_\ell| < 0.8 . \quad (6)$$

The mass cut largely eliminates the leading background from $e^+e^- \rightarrow W^+W^-$ and the polar angle cut helps reduce the other large background from $e^+e^- \rightarrow ZZ$. Since the Z boson in the signal is not only central, but also energetic with $E_Z = (s - m_h^2 + m_Z^2)/2\sqrt{s} \approx \sqrt{s}/2$, we can further reduce the background by imposing a cut of

$$p_T(e^+e^-) > 80 \text{ GeV} . \quad (7)$$

The signal to background ratio is improved after the cuts to the extent that the Higgs must be nearly degenerate with the Z for the M_{rec} peak to have any significant background. Figure 2 presents the recoil mass distributions, $d\sigma/dM_{\text{rec}}$, for $e^+e^- \rightarrow e^+e^-X$ at $\sqrt{s} = 500$ GeV. Results for different energy/momentum resolutions, cases I-IV, are shown in the four different panels. The solid and dashed curves give the Zh signal for $m_h = 90$ and 120 GeV, respectively. The dotted line is the summed SM background.

The $e^+e^- \rightarrow Zh$ cross section reaches a maximum near $\sqrt{s} \sim m_Z + \sqrt{2} m_h$. A relevant question is how much improvement is possible by running the machine at a lower energy nearer the maximum cross section, as would be possible once m_h is known (either from LHC or NLC data). To illustrate, we consider $\sqrt{s} = 250$ GeV. Figure 3 shows the recoil mass distributions, $d\sigma/dM_{\text{rec}}$, similar to those in Fig. 2

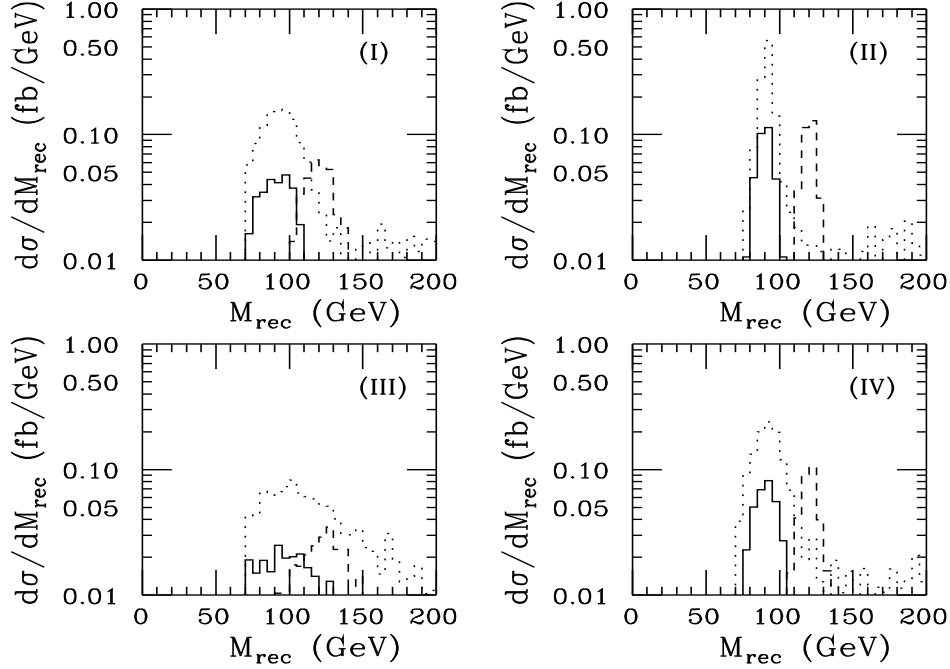


Figure 2: Recoil mass distributions for $e^+e^- \rightarrow e^+e^-X$ at $\sqrt{s} = 500$ GeV. The solid and dashed curves give the Zh signal for $m_h = 90$ and 120 GeV, respectively. The dotted line is the summed SM background. Results for the different energy/momentum resolution, cases I-IV, are shown in the four different panels. The cuts of Eqs. (5), (6) and (7) have been imposed.

but for $\sqrt{s} = 250$ GeV. We see not only that the cross section rate is larger, but also that the signal peak is much sharper because of the better determination for lepton energy/momentum at this lower \sqrt{s} .

We estimate the relative statistical error for the cross section measurement as

$$R = \sqrt{S+B}/S, \quad (8)$$

where S and B are the numbers of signal and background events for a given luminosity; neglecting systematic uncertainty from correcting for our cuts, this is also the error on the coupling g_{ZZh}^2 . In Table 1 we compare the accuracy achieved (as a function of m_h) in the Zh mode, with $Z \rightarrow e^+e^-$, for different resolution choices, taking $\sqrt{s} = 500$ GeV and 250 GeV and assuming an integrated luminosity of $L = 200 \text{ fb}^{-1}$. At $\sqrt{s} = 500$ GeV, the accuracy ranges from $\sim 15\%$ at $m_h = 80$ GeV to $\sim 7\%$ at $m_h = 140$ GeV. In general, the accuracy is not greatly affected by the detector. The exception is case III which yields poorer results than the other cases. Results for the g_{ZZh}^2 accuracy at $\sqrt{s} = 250$ GeV are $\sim 6\%$ (more or less independent of resolution choice) for most values of m_h , worsening to $\sim 7\%$

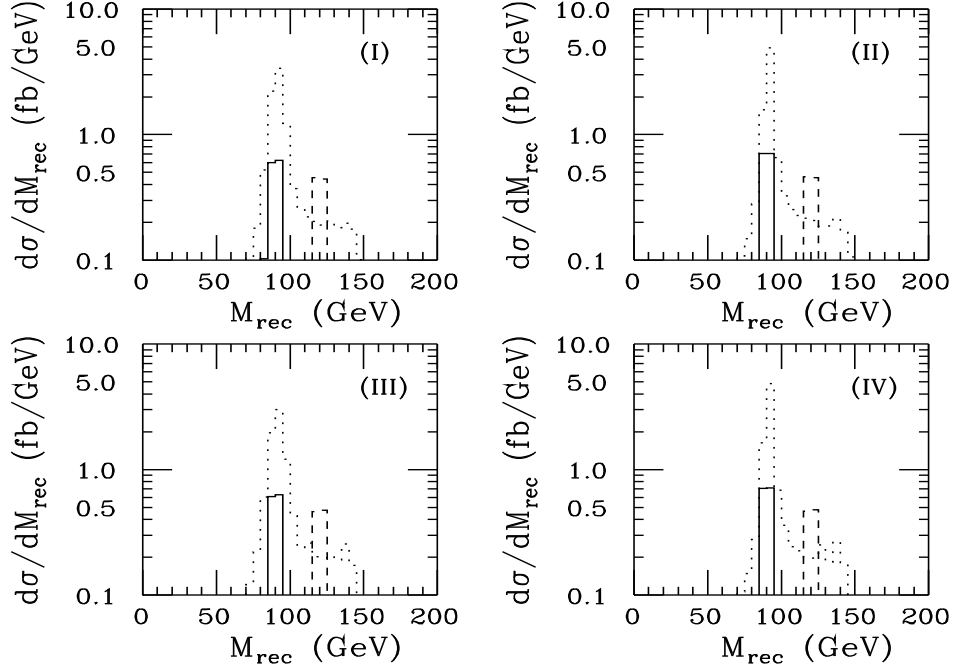


Figure 3: Recoil mass distributions for $e^+e^- \rightarrow e^+e^-X$ at $\sqrt{s} = 250$ GeV. The solid and dashed curves give the Zh signal for $m_h = 90$ and 120 GeV, respectively. The dotted line is the summed SM background. Results for the different energy/momentum resolution, cases I-IV, are shown in the four different panels. The cuts of Eqs. (5) and (6) have been imposed.

at the Z peak. Thus, by running the machine at an energy near the maximum in the Zh cross section we are able to improve the accuracy for this particular mode by about a factor of 2.

We compute the net accuracy for the g_{ZZh}^2 measurement in the Zh channel by including measurements for both the $Z \rightarrow e^+e^-$ and the $Z \rightarrow \mu^+\mu^-$ final states. The net error (R_{net}) is given by

$$R_{\text{net}}^{-2} = R_e^{-2} + R_\mu^{-2}. \quad (9)$$

In obtaining the error for the e^+e^- final state, we compare results found using the EM calorimeter to those found using tracking and adopt the superior choice. Thus, for example, if we assume NLC/EM and NLC/tracking, this means using case I results for the $Z \rightarrow e^+e^-$ final state and case III results for the $Z \rightarrow \mu^+\mu^-$ final state. The results are illustrated in Table 2. We see that at $\sqrt{s} = 250$ GeV an accuracy for g_{ZZh}^2 of less than 5% can be reached.⁴

⁴This, and other results obtained here for the Zh mode are generally consistent with those

Table 1: Percentage accuracy for g_{ZZh}^2 based on Zh channel $e^+e^- \rightarrow e^+e^-h$ cross section measurements with $L = 200 \text{ fb}^{-1}$ assuming (a) $\sqrt{s} = 500 \text{ GeV}$ and (b) $\sqrt{s} = 250 \text{ GeV}$. Results for the four different lepton energy/momentum resolutions are shown. The cuts of Eqs. (5) and (6) have been imposed for both $\sqrt{s} = 500 \text{ GeV}$ and $\sqrt{s} = 250 \text{ GeV}$. For $\sqrt{s} = 500 \text{ GeV}$ we have imposed the additional cut (7). Note that only one kind of lepton is counted here.

(a) $\sqrt{s} = 500 \text{ GeV}$						
resolution	mass bin	$m_h (\text{ GeV})$				
		80	90	100	120	140
I	$(m_h \pm 10)$	15%	15%	12%	8.3%	7.2%
II	$(m_h \pm 10)$	11%	12%	10%	6.2%	6.4%
III	$(m_h \pm 10)$	19%	21%	18%	15%	12%
IV	$(m_h \pm 10)$	11%	12%	10%	6.8%	6.5%
(b) $\sqrt{s} = 250 \text{ GeV}$						
I	$(m_h \pm 10)$	5.7%	6.7%	6.3%	4.8%	6.6%
II	$(m_h \pm 10)$	5.8%	6.8%	6.7%	4.8%	6.5%
III	$(m_h \pm 10)$	5.6%	6.7%	6.7%	4.7%	6.7%
IV	$(m_h \pm 10)$	5.8%	6.7%	6.7%	4.7%	6.7%

Table 2: The percentage accuracy for g_{ZZh}^2 obtained by combining [via Eq. (9)] results for the Zh cross section measurement in the $e^+e^- \rightarrow e^+e^-h$ (NLC/EM) channel and the $e^+e^- \rightarrow \mu^+\mu^-h$ (NLC/tracking) channel, assuming $L = 200 \text{ fb}^{-1}$ and $\sqrt{s} = 500 \text{ GeV}$ or $\sqrt{s} = 250 \text{ GeV}$. The cuts of of Eqs. (5) and (6) have been imposed for both energies and for $\sqrt{s} = 500 \text{ GeV}$ we impose the additional cut (7). The mass bins of Table 1 have been employed.

$\sqrt{s} (\text{ GeV})$	$m_h (\text{ GeV})$				
	80	90	100	120	140
500	12%	12%	10%	7.3%	6.2%
250	4.0%	4.7%	4.6%	3.4%	4.7%

2.2 $e^+e^- \rightarrow e^+e^-h$ and $e^-e^- \rightarrow e^-e^-h$ via ZZ -fusion

The major advantage for the ZZ -fusion channel (2) over the Zh channel (1) is that the cross section increases logarithmically with energy; at $\sqrt{s} = 500$ GeV and for $m_h = 120$ GeV it is about 10 fb as compared to the Zh cross section of about 2.5 fb. To remove the large ZZ background, we require, in addition to the basic cuts of Eq. (5),

$$M_{ee} > 100 \text{ GeV} . \quad (10)$$

The only penalty from the M_{ee} cut is a 20% decrease in the signal rate due to elimination of the constructive interference of the ZZ -fusion amplitude with the Zh amplitude.

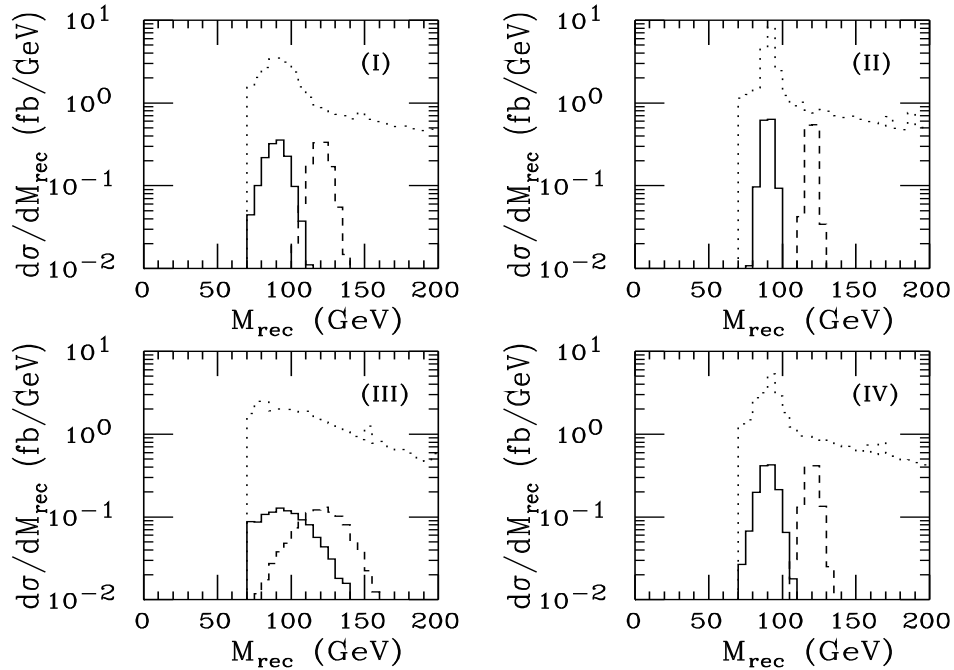


Figure 4: Recoil mass distributions for $e^+e^- \rightarrow e^+e^-X$ at $\sqrt{s} = 500$ GeV. Results for $m_h = 90$ GeV (solid), and 120 GeV (dashed) are shown. Results for the different energy/momentum resolution, cases I-IV, are shown in the four different panels. We impose the cuts of Eqs. (5) and (10).

Figure 4 presents signal and background curves after the cuts of Eqs. (5) and (10). Although some background persists,⁵ the much larger signal rate makes of Refs. [6, 7, 2, 9] for $m_h \gtrsim 110$ GeV, when the same electromagnetic-calorimeter/tracking resolution assumptions are made. For lower m_h , we find higher backgrounds as compared to the estimates made in Ref. [2], resulting in larger errors.

⁵The signal-to-background ratio can be further enhanced by stronger cuts, but the signal rate is also reduced and the error in the measurement of g_{ZZh}^2 is not improved.

Table 3: Percentage accuracy for g_{ZZh}^2 based on the ZZ -fusion channel $e^+e^- \rightarrow e^+e^-h$ cross section measurements with $L = 200 \text{ fb}^{-1}$ at $\sqrt{s} = 500 \text{ GeV}$. Results for NLC/EM, CMS/EM and SJLC/tracking (resolution cases I, II and IV) are shown; NLC/tracking yields much poorer results than NLC/EM. The cuts of Eqs. (5), and (10) have been imposed.

$\sqrt{s} = 500 \text{ GeV}$						
resolution	mass bin	$m_h (\text{ GeV})$				
		80	90	100	120	140
I	$(m_h \pm 10)$	9.7%	10%	9.6%	6.9%	7.2%
II	$(m_h \pm 10)$	8.8%	9.7%	11%	6.3%	6.8%
III	$(m_h \pm 10)$	19%	18%	17%	15%	14%
IV	$(m_h \pm 10)$	9.1%	9.9%	9.2%	6.6%	7.0%

Table 4: Combined percentage accuracy for g_{ZZh}^2 as obtained by including the three measurements: $e^+e^- \rightarrow e^+e^-h$ for the Zh and ZZ -fusion (NLC/EM) plus $e^+e^- \rightarrow \mu^+\mu^-h$ for the Zh (NLC/tracking) at $\sqrt{s} = 500 \text{ GeV}$ and $L = 200 \text{ fb}^{-1}$. Cuts as specified in Tables 1 and 3 are imposed.

$m_h (\text{ GeV})$				
80	90	100	120	140
7.5%	7.7%	6.9%	5.0%	4.7%

a good measurement of the cross section feasible. The corresponding results for the accuracy of the g_{ZZh}^2 measurement are presented in Table 3. Using NLC/EM calorimetry, case I, the accuracy ranges from 10% to 7%. As in the Zh channel, there is little difference between results for the resolution cases I, II and IV, whereas case III yields substantially poorer results.

The ultimate accuracy that can be obtained for g_{ZZh}^2 at $\sqrt{s} = 500 \text{ GeV}$ is obtained by combining the Zh and ZZ -fusion channel results. In Table 4, we present this accuracy as a function of m_h , assuming that NLC/EM energy resolution is employed for the e^+e^-h final states of the Zh and ZZ -fusion channels and that NLC/tracking resolution is employed for the $\mu^+\mu^-h$ final state of the Zh channel. Note that the achievable accuracy is competitive with that obtained at $\sqrt{s} = 250 \text{ GeV}$ using the Zh mode alone (the ZZ -fusion mode being not useful at this low energy), especially at the larger m_h values.

At an e^-e^- collider, Higgs production is entirely from the ZZ -fusion process, $e^-e^- \rightarrow e^-e^-h$. The results presented in Table 3 are essentially applicable, except that the background level is slightly smaller in the e^-e^- case [5].

3 Summary and Conclusions

We have investigated the precision with which the Higgs boson to ZZ coupling (g_{ZZh}^2) can be measured by employing the recoil mass distribution in $\ell^+\ell^-h$ ($\ell = e, \mu$) final states coming from the Zh and ZZ -fusion production channels at an e^+e^- collider or ZZ -fusion (alone) at an e^-e^- collider. From the (fully inclusive) recoil mass distribution a direct determination of g_{ZZh}^2 , that is independent of any assumptions regarding the branching ratio for the Higgs boson to decay into any particular channel, can be made. We considered a number of electromagnetic calorimetry and tracking resolution options for the detector. Results for the four options considered are similar, except that the tracking specified for the ‘typical’ NLC detector yields poor results at $\sqrt{s} = 500$ GeV. For the calorimetry and tracking resolutions specified for this typical NLC detector, we find the following results for the accuracy of the g_{ZZh}^2 measurement for m_h in the range 80–140 GeV:

- If the e^+e^- collider is run at $\sqrt{s} = 500$ GeV, the ZZ -fusion production mode yields smaller statistical error than does the Zh production mode (even after combining both e^+e^-h and $\mu^+\mu^-h$ final states in the latter case).
- Taking both Zh channel and ZZ -fusion channel measurements at $\sqrt{s} = 500$ GeV and 200 fb^{-1} into account, the combined accuracy is predicted to range from 7.5% at $m_h = 80$ GeV to 4.7% at $m_h = 140$ GeV (Table 4).
- Running at a lower energy near the Zh cross section maximum is possibly fruitful. For accumulated luminosity of 200 fb^{-1} at $\sqrt{s} = 250$ GeV, the accuracy achieved using the (dominant) Zh production mode is less than 5% for $80 \leq m_h \leq 140$ GeV (Table 2).
- The statistical accuracy of a measurement in the ZZ -fusion $e^-e^- \rightarrow e^-e^-h$ channel would be somewhat better than that for a measurement in the ZZ -fusion $e^+e^- \rightarrow e^+e^-h$ channel (Table 3), due to smaller backgrounds.

The most significant implication of our results is that it may not be necessary, or even appropriate, to run at low energy in order to obtain the best possible accuracy for the g_{ZZh}^2 measurement. When running at the full energy of $\sqrt{s} = 500$ GeV, if $m_h \gtrsim 120$ GeV then (for NLC/EM and NLC/tracking) the combined Zh and ZZ -fusion error of Table 4 is very close to that obtained when running at $\sqrt{s} = 250$ GeV *for the same integrated luminosity*. Further, it seems likely that it will prove desirable from the point of view of other physics to accumulate more luminosity at $\sqrt{s} = 500$ GeV than at $\sqrt{s} = 250$ GeV, and it is also possible [13] that the instantaneous luminosity at the lower energy will be lower (assuming that the interaction region is optimized initially for $\sqrt{s} = 500$ GeV). In either case, the lower energy running might not significantly improve the g_{ZZh}^2 accuracy even if $m_h < 120$ GeV.

Thus, we conclude that use of the ZZ -fusion mode (as well as the Zh mode) will provide a very valuable increase in the accuracy that can be achieved for the measurement of the ZZ coupling of a SM-like Higgs boson at a lepton collider operating at high energy.

4 Acknowledgements

This work was supported in part by the DOE under contracts No. DE-FG03-91ER40674 and No. DE-FG02-95ER40896, and in part by the Davis Institute for High Energy Physics.

References

- [1] J.F. Gunion, A. Stange, and S. Willenbrock, *Weakly-Coupled Higgs Bosons*, UCD-95-28 (1995), published in *Electroweak Physics and Beyond the Standard Model*, World Scientific Publishing Co., eds. T. Barklow, S. Dawson, H. Haber, and J. Siegrist, pp. 23–145.
- [2] J.F. Gunion, L. Poggioli, R. Van Kooten, C. Kao and P. Rowson, in *New Directions for High-Energy Physics*, Proceedings of the 1996 DPF/DPB Summer Study on High-Energy Physics, June 25—July 12, 1996, Snowmass, CO, edited by D.G. Cassel, L.T. Gennari, and R.H. Siemann (Stanford Linear Accelerator Center, 1997), pp. 541–587.
- [3] J. F. Gunion, H. Haber, and J. Wudka, Phys. Rev. **D43**, 904 (1991).
- [4] We have made use of the Helicity Amplitude package, MadGraph by T. Stelzer and W. Long, Comput. Phys. Commun. **81**, 357 (1994).
- [5] V. Barger, J. Beacom, K. Cheung, and T. Han, Phys. Rev. **D50**, 6704 (1994); T. Han, Int. Journ. Mod. Phys. **A11**, 1541 (1996).
- [6] P. Janot, *Proceedings of the 2nd International Workshop on “Physics and Experiments with Linear e^+e^- Colliders”*, eds. F. Harris, S. Olsen, S. Pakvasa and X. Tata, Waikoloa, HI (1993), World Scientific Publishing, p. 192.
- [7] K. Kawagoe, *Proceedings of the 2nd International Workshop on “Physics and Experiments with Linear e^+e^- Colliders”*, eds. F. Harris, S. Olsen, S. Pakvasa and X. Tata, Waikoloa, HI (1993), World Scientific Publishing, p. 660.
- [8] *Physics and Technology of the Next Linear Collider: a Report Submitted to Snowmass 1996*, BNL 52-502, FNAL-PUB-96/112, LBNL-PUB-5425, SLAC Report 485, UCRL-ID-124160.

- [9] *Physics with e^+e^- Colliders*, by ECFA/DESY LC Physics Working Group (E. Accomando, *et al.*), hep-ph/9705442.
- [10] P. Minkowski, presentations at the U.C. Santa Cruz Workshops on e^-e^- Colliders.
- [11] CMS Technical Proposal, CERN/LHCC 94-38.
- [12] See “JLC-I”, KEK-92-16, December 1992; private communication with R. Van Kooten.
- [13] J. Irwin, private communication.